Research Square

Preprints are preliminary reports that have not undergone peer review.
They should not be considered conclusive, used to inform clinical practice,
or referenced by the media as validated information.

Computer simulation of retrogradely propagated action currents and potentials recorded in the rat cerebellar granule cell, and model estimation of Na + and K + ion concentration change

Armuntas Baginskas

armuntas.baginskas@lsmuni.lt

Lithuanian University of Health Sciences

George William Balagana

Lithuanian University of Health Sciences

Research Article

Keywords: parallel fiber, action current, resurgent current, action potential, ADC, ADP

Posted Date: April 28th, 2026

DOI: https://doi.org/10.21203/rs.3.rs-9086443/v1

License: This work is licensed under a Creative Commons Attribution 4.0 International License.
Read Full License

Additional Declarations: No competing interests reported.

Computer simulation of retrogradely propagated action currents and potentials recorded in the rat cerebellar granule cell, and model estimation of Na^+ and K^+ ion concentration change

Armuntas Baginskas, George William Balagana
[a]Department of Physics, Mathematics and Biophysics, Lithuanian University of Health Sciences, Eiveniu 4, Kaunas LT 50161, Lithuania

Corresponding author:
A. Baginskas,
Department of Physics, Mathematics and Biophysics,
Lithuanian University of Health Sciences,
Eiveniu 4, Kaunas LT 50161,
Lithuania
ORCID iD 0000-0002-3111-6087

Phone: (370 37) 327327
E-mail: armuntas.baginskas@lsmuni.lt

Running title: **Computer simulation of retrogradely propagated …**

Number of pages: 35
Number of figures: 11
Number of tables: 3

Abbreviations. AC – action current, AP – action potential, ADC – afterdepolarizing current, ADP – afterdepolarization potential, AHC – afterhyperpolarizing current, AHP – afterhyperpolarization potential

Abstract

Retrogradely propagated action currents and potentials were recorded in the rat cerebellar granule cells. The action currents consisted of the fast transient, having amplitude and width of -294 ± 27 pA, 0.73 ± 0.04 ms, followed by the slower transient – afterdepolarizing current (ADC), having amplitude and duration of -9.65 ± 2.45 pA, 9.16 ± 0.51 ms. Amplitude and width of the soma-recording site RC circuit filtered action potentials were equal to 12.4 ± 1.24 mV, 23.17 ± 2.49 ms.

The recorded action currents and potentials were computer simulated in the model cell of real geometry. Modeled action currents and potentials matched the recorded ones when maximal density of the fast sodium conductance in the cerebellar parallel fibers was equal to 81 mS/cm^2, maximal density of delayed rectifier potassium conductance was equal to 45 mS/cm^2, and the density of resurgent sodium conductance comprised 1% of the fast sodium conductance.

The modeling showed that afterdepolarising current (ADC) is a sum of the resurgent sodium current and delayed rectifier potassium current, and afterdepolarization potential (ADP) is a sum of depolarization, caused by the resurgent sodium current, and afterhyperpolarization, caused by the delayed rectifier potassium current.

The change of sodium and potassium ion concentration in the parallel fibers was calculated to be equal to 27.63 mM, -28.01 mM at 22º C, and 13.69 mM, -14.08 mM at 37º C due to propagation of 20 spikes long trains – large enough to affect biochemical and electrical processes in the cell.

Keywords

parallel fiber; action current; resurgent current; action potential; ADC; ADP

Declarations

Funding: No funds, grants, or other support was received.

Conflicts of interest/Competing interests: The authors declare that they have no conflict of interest.

Availability of data and material: All the data of the study are freely available and can be delivered on request by the corresponding author Armuntas Baginskas.

Code availability: Not applicable.

Authors' contributions: The part of the author Armuntas Baginskas in the experiments, analysis, discussion, interpretation of the experimental results, and manuscript writing constitutes 95%, and of the author Balagan – 5% of the entire work. The authors have approved the final text of the manuscript.

Ethics approval: Not applicable.

Consent to participate: Not applicable.

Consent for publication: Not applicable.

Introduction

Parallel fibers of the cerebellar granule cells are very thin, measuring of 0.15-0.3 μm in diameter (Pichitpornchai et al., 1994; Su et al., 1996; Gundappa-Sulur et al., 1999; Huang et al. 2006; Dover et al., 2016), precluding direct measurement of sodium-potassium current and evaluation of sodium and potassium conductance (channels) densities in the parallel fibers. It is possible, however, to record in the granule cell soma retrogradely propagated action currents and potentials evoked in the parallel fiber far away from the soma. Since the cerebellar granule cell soma and dendrites do not have spike-generating channels (do not fire action potentials) (Masoli et al., 2017, 2020; Schaller and Caldwell, 2003; Diwakar et al., 2009; Osorio et al., 2025), computer simulation of the shape, amplitude, duration, latency, velocity, highest transmitted frequency of the action currents and potentials gives a possibility to estimate the spike-generating conductance (channels) densities in the parallel fibers. This is the **first objective** of the present work.

The **second objective** is to estimate change of sodium and potassium ion concentrations in the parallel fibers, caused by the propagation of action potentials in the model cell. This is not a trivial question due to a small size of parallel fibers. The small size can cast a challenge to a common belief that transmembrane ion currents do not change intracellular ion concentrations appreciably. Since surface-to-volume ratio increases with decrease of axon diameter, the diameter lastly will be reached that transmembrane currents already appreciably change intra-axonal ion concentrations. The increased sodium ion concentration can lead to physiological effects: alter resting membrane potential, neuron excitability, conduction velocity (Tigerholm et al., 2015; Zylbertal et al., 2017), enhance Ca^{2+} ion influx through NMDA receptors and Na^{+}/Ca^{2+} exchangers (Wasman, 2006; Yu et al., 2010). Sodium ions serve as second messenger particles,

targeting the activity of some proteases, kinases, and membrane G-proteins (Page and Di Cera, 2006; Ono et al., 2010; Wang et al., 2016). Trains of 20 spikes with a frequency of up to 1 kHz are evidenced in the cerebellar granule cells by Jorntell and Ekerot (2006), Rancz et al. (2007), van Beugen et al. (2013), Powell et al. (2015), and it is of interest to evaluate change of sodium and potassium ion concentration during them.

Methods

Experimental procedure

Experiments were performed *in vitro* with nine 17-26 days old Wistar rats. Requirements of the "Principles of laboratory animal care" (NIH publication No. 86-23), and of European Communities Council Directive 86/609/EEC were fulfilled in the experiments.

Rats were anesthetized, decapitated and their brains were taken out and kept for a while in an icy cold oxygenated dissection solution, then moved to the slicing bath. The cerebellum was cut up in parallel to its base into a few 400 μm thick slices afterwards stored at room temperature in the oxygenated extracellular solution. The composition of the solutions used in the experiments was as follows: dissection solution – KCl 1.25 mM, $CaCl_2$ 0.5 mM, $MgCl_2$ 7 mM, $NaHCO_3$ 25 mM, KH_2PO_4 1.25 mM, glucose 16 mM, glycerol 250 mM; extracellular (perfusion) solution – NaCl 125 mM, KCl 1.25 mM, $CaCl_2$ 2 mM, $MgCl_2$ 1 mM, $NaHCO_3$ 25 mM, KH_2PO_4 1.25 mM, glucose 16 mM; intracellular (recording pipette) solution – K-gluconate 120 mM, KCl 18 mM, $MgCl_2$ 2 mM, NaCl 2 mM, Na_2ATP 2 mM, HEPES 10 mM.

Slice has been then transferred into the recording bath full of the circulating oxygenated extracellular solution at the temperature of 22^o C, and the stimulating and recording electrodes were positioned in the slice, for recording of retrogradely propagated action currents and potentials. Arrangement of electrodes are shown in Figure 1.

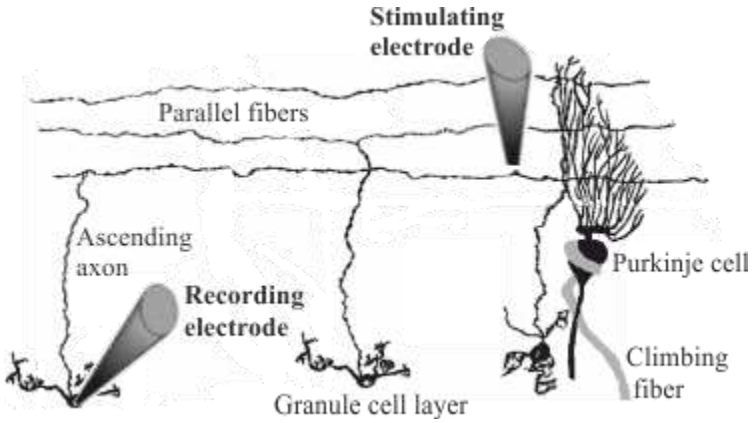


Fig. 1. Schematic view of the cerebellar cortex, and arrangement of the electrodes in the experiment.

Recording microelectrode (pipette), filled with the intracellular solution and having resistance of ~8 MΩ, was brought into the granule cell layer of cerebellum. Whole cell patch clamp was achieved with one of the granule cells and cell accessed.

Stimulating pipette, filled with the extracellular solution and having resistance of ~1.5 MΩ, was brought into the parallel fiber layer at a distance in the range of 0.5 mm to 1 mm (average distance 0.75 mm) from the recording microelectrode. The distance was roughly estimated by eye. Voltage pulses of amplitude of 20–60 V and duration of 50 μs were applied through the stimulating electrode to excite the parallel fibers, using *npi* stimulator *ISO-STIM 01M*. The stimulating pipette has been slightly moving to secure the response in the accessed cell.

Retrogradely propagated action currents and potentials were recorded using *npi* single electrode switching VC, CC amplifier *SEC-10LX* set to the voltage clamp (VC) mode for recording of action currents, and to the current clamp (CC) mode for recording of action potentials. Amplitude, width, and latency of the recorded responses were measured. Amplitude was measured as height of the response from the base line till the peak, width – as thickness of the response at half amplitude level, latency – as time interval from the stimulus artifact till maximum of the response. Values are presented as mean ± SE.

The recordings were done at the ambient temperature of ~22° C with the synaptic blockers KYNA (1 mM), CNQX (20 μM), and picrotoxin (25 μM) in the perfusion solution. The chemicals were purchased from Sigma-Aldrich Co.

Modeling procedure

The model of granule cell reproduces a real geometry of rat cerebellar granule cell taken from the work of Arleo et al. (2010) (figure 1 in their article). Morphometric and electrical parameters of the model granule cell are shown in Figure 2.

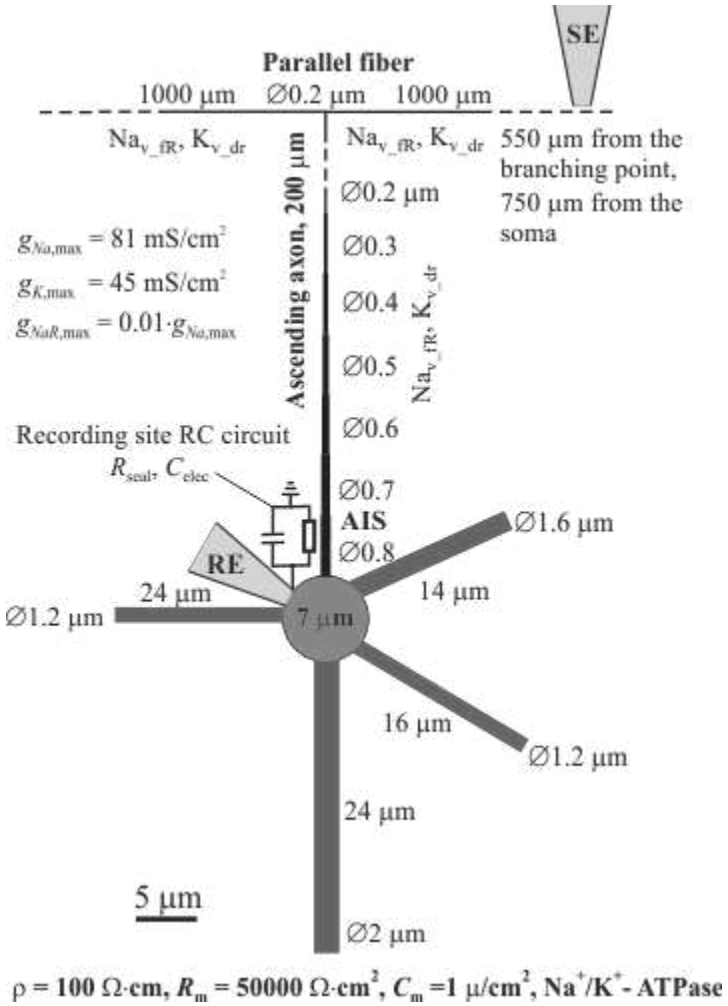


Fig 2. Model of the granule cell. AIS – axon initial segment, RE – recording electrode, SE – stimulating electrode, ρ – resistivity of intracellular medium, R_m – membrane specific resistance, C_m – membrane specific capacitance, R_{seal} – resistance of the whole cell patch clamp, C_{elec} – not fully compensated capacitance of the recording system. Na^+/K^+-ATPase is embedded in the membrane of entire model cell. Na_{v_fR} – fast voltage-gated sodium channels having a property of generation of resurgent current, K_{v_dr} – delayed rectifier voltage-gated potassium channels. Spike generating Na_{v_fR} and K_{v_dr} channels are embedded in the membrane of ascending axon and parallel fibers. $g_{Na,max}$ – maximal density of the fast sodium conductance, $g_{K,max}$ – maximal density of the delayed rectifier potassium conductance, $g_{NaR,max}$ – maximal density of the resurgent sodium conductance.

Soma and dendrites of the model cell are considered passive, i. e. they do not have spike-generating channels. Absence of these channels in the soma-dendritic membrane of cerebellar granule cells was demonstrated in the studies of Schaller and Caldwell (2003), Diwakar et al. (2009), Masoli et al. (2020), Osorio et al. (2025). Ascending axon and parallel fibers are considered active, i. e. they have spike-generating channels.

Passive electrical parameters of the model cell are set to be identical for the entire cell and equal to the regular values: resistivity of intracellular medium $\rho = 100$ Ω·cm, specific resistance of the plasma membrane $R_m = 50000$ Ω·cm^2, specific capacitance of the plasma membrane $C_m = 1$ μF/cm^2 (see, for example, Diwakar et al., 2009).

Sodium-potassium pump (Na^+/K^+-ATPase) are embedded in the entire membrane of the model cell. The density of ionic current generated by the pump is modeled by the equation taken from the work of Chizhov et al. (2019)

$$j_{pump} = \frac{j_{pump,max}}{(1+e^{3.5-K_o})\cdot(1+e^{(20.5-Na_i)/3})}, \quad (1)$$

where j_{pump} is density of the sodium pump current, K_o and Na_i are extracellular concentration of K^+ ions and intracellular concentration of Na^+ ions in mM, $j_{pump,max}$ – maximal density of the pump current at the room temperature of 20 °C equal to 10^{-4} nA/μm^2.

Spike-generating fast voltage-gated sodium channels having a property of generation of resurgent current (Lewis and Raman, 2014), Na_{v_fR}, and delayed rectifier voltage-gated potassium channels, K_{v_dr}, are present in the ascending axon and parallel fiber membrane. The ionic currents through these channels have been modeled by using Hodgkin-Huxley formalism (Liu et al., 1998; Gerstner et al., 2014; Fohlmeister, 2015; Fang et al., 2021; Zang et al., 2023)

$$\begin{aligned} j_{Na} &= g_{Na,\max} \cdot m^3 \cdot h \cdot (V_m - E_{Na}), \\ j_K &= g_{K,\max} \cdot n^4 \cdot (V_m - E_K), \end{aligned} \tag{2}$$

where j_{Na}, j_K are densities of the fast sodium and delayed rectifier potassium currents, $g_{Na,\max}$, $g_{K,\max}$ – maximal densities of the fast sodium and delayed rectifier potassium conductance, E_{Na}, E_K – sodium and potassium ion reversal potentials, calculated using the Nernst equation from the extracellular and intracellular ion concentrations, V_m – transmembrane potential, m, n, h – gate variables (probabilities of Na^+ and K^+ channel gates to be in the open state) obeying the kinetic equations

$$\begin{aligned} \frac{\mathrm{d}m}{\mathrm{d}t} &= \alpha_m \cdot (1-m) - \beta_m \cdot m, \\ \frac{\mathrm{d}h}{\mathrm{d}t} &= \alpha_h \cdot (1-h) - \beta_h \cdot h, \\ \frac{\mathrm{d}n}{\mathrm{d}t} &= \alpha_n \cdot (1-n) - \beta_n \cdot n, \end{aligned} \tag{3}$$

where α_m, α_h, α_n are opening rate constants, and β_m, β_h, β_n are closing rate constants, which depend on the temperature and the transmembrane voltage V_m. The dependence of the rate constants on the V_m at the room temperature of 20° C is expressed by the following equalities:

$$\begin{aligned}
&\alpha_m(V_m) = \frac{1.74\cdot(V_m-11)}{1-e^{-\frac{V_m-11}{12.94}}}, \quad \beta_m(V_m) = -\frac{0.06\cdot(V_m-5.9)}{1-e^{\frac{V_m-5.9}{4.47}}};\\
&\alpha_h(V_m) = 3\cdot e^{-\frac{V_m+80}{10}}, \qquad \beta_h(V_m) = \frac{12}{1+e^{-\frac{V_m-77}{27}}};\\
&\alpha_n(V_m) = \frac{0.018\cdot V_m}{1-e^{-\frac{V_m}{25}}}, \qquad \beta_n(V_m) = -\frac{0.0036\cdot(V_m-10)}{1-e^{\frac{V_m-10}{12}}}.
\end{aligned} \tag{4}$$

The resurgent sodium current is modeled as follows: At the end of the inactivation process of fast sodium channels, when 90% of the *h* gates get closed, one hundredth (~1%) fraction of the fast sodium channels quickly, within ~0.1 ms, enter a slow inactivation mode (state) with a characteristic inactivation time equal to ~10 ms. Based on the results of studies of Afshari et al. (2004), Fatemeh et al. (2004); Magistrettti et al. (2006), Diwakar et al. (2009), Lewis and Raman (2014), Aman and Raman (2024), the resurgent current has been modelled with the following equation:

$$j_{NaR} = g_{NaR,\max}\cdot(1-e^{-\frac{t-t_a}{\tau_{ac}}})\cdot e^{-\frac{t-t_a}{\tau_{in}}}\cdot(V_m-E_{Na}), \tag{5}$$

where j_{NaR} is density of the resurgent sodium current, $g_{NaR,\max}$ – maximal density of the resurgent sodium conductance, set to 1% of maximal density of the fast sodium conductance, i. e. $g_{NaR,\max} = 0.01\cdot g_{Na,\max}$, t_a – time of activation of the resurgent sodium current, approximately equal to the

time moment when 90% of the fast sodium channels get inactivated (90% of h gates close), τ_{ac} and τ_{in} – activation and inactivation time constants at the room temperature of 20 ºC equal to 0.05 ms, and 6 ms, respectively, V_m – transmembrane potential, E_{Na} – reversal potential of the sodium ions.

Temperature dependence of opening and closing rate constants, and Na^+/K^+-ATPase turnover rate is described by using Q_{10} factor approach. This factor quantifies, how many times the rate of biochemical processes increases with 10º C increase in temperature. It is acknowledged, that for most of biological and biochemical processes $Q_{10} \approx 2$ in the range of temperatures from 20º C to 40º C (Steratt, 2015). Therefore, if at the temperature of t_0º rate of biochemical process is R_0, then at the temperature of tº it will be

$$R = R_0 \cdot Q_{10}^{\frac{t^o - t_0^o}{10}} = R_0 \cdot 2^{\frac{t^o - t_0^o}{10}}. \quad (6)$$

Sodium and potassium ions diffuse along axons and dendrites with the diffusion coefficients of 1.2 μm^2/ms for Na^+, and 2 μm^2/ms for K^+ ions, measured in the study of Wang et al. (2025).

Extracellular concentrations of ions are set to be equal to the values used in the experiments Na_o = 150 mM, K_o = 2.5 mM, Cl_o = 132 mM, Ca_o = 2 mM. Intracellular concentrations of ions are set to be equal to the regular values for cerebellar granule cells (see, for example, Chen et al., 1999) Na_{i0} = 8 mM, K_{i0} = 155 mM, Cl_i = 132 mM, Ca_i = 2 nM. Resting potential calculated using Goldman-Hodgkin-Katz equation is equal to -73.12 mV.

The soma has been modelled as an equipotential sphere of a diameter of 7 μm with passive electrical parameters R_m = 50000 Ω·cm^2, C_m = 1 μF/cm^2.

The whole cell patch clamp (recording site in the soma) has been modeled as RC circuit composed of seal resistance, R_{seal}, and recording system capacitance, C_{elec}. The recording site RC circuit connects in parallel to the soma RC circuit.

The site of stimulation is positioned at the distance of 750 μm from the soma along the ascending axon and parallel fiber path as it was in the experiments.

The dendrites, ascending axon and parallel fibers are divided into 5 μm length compartments. The finite difference equations for each of the compartment are written and solved by the Crank-Nicolson-Newton method. This multicompartmental algorithm was implemented into C++ language program used to compute action currents and potentials, and estimate Na^+, K^+ ion concentration change caused by the propagation of action potentials.

Two parameters – maximal density of the fast sodium conductance ($g_{Na,max}$), and maximal density of the delayed rectifier potassium conductance ($g_{K,max}$) – has been changing to match the modeled and recorded action currents. Based on the results of the work of Wen et al. (2019), the reasonable values of the parameters to start the simulation have been chosen as follows, $g_{Na,max}$ = 100 mS/cm^2, $g_{K,max}$ = 50 mS/cm^2. Additional two parameters – whole cell patch clamp seal resistance (R_{seal}) and recording system capacitance (C_{elec}) – have been changing to match modeled and recorded action potentials. Based on the results of the studies of Sigworth (1995), and Polder et al. (2006), the patch clamp recording system capacitance C_{elec} is in the range of 10-15 pF, and the seal resistance R_{seal} of fair whole cell patch clamp is equal to ~1 GΩ.

Results

Recordings of action currents and potentials

The recordings of retrogradely (antidromically) propagated action currents (AC) and potentials (AP) have been achieved from 12 granule cells of the cerebellum of 9 rats. Examples of the recorded traces together with the computer simulated trace are shown in Figure 3. Traces of the recorded action currents exhibit a fast transience followed by a slow transience – afterdepolarizing current (ADC).

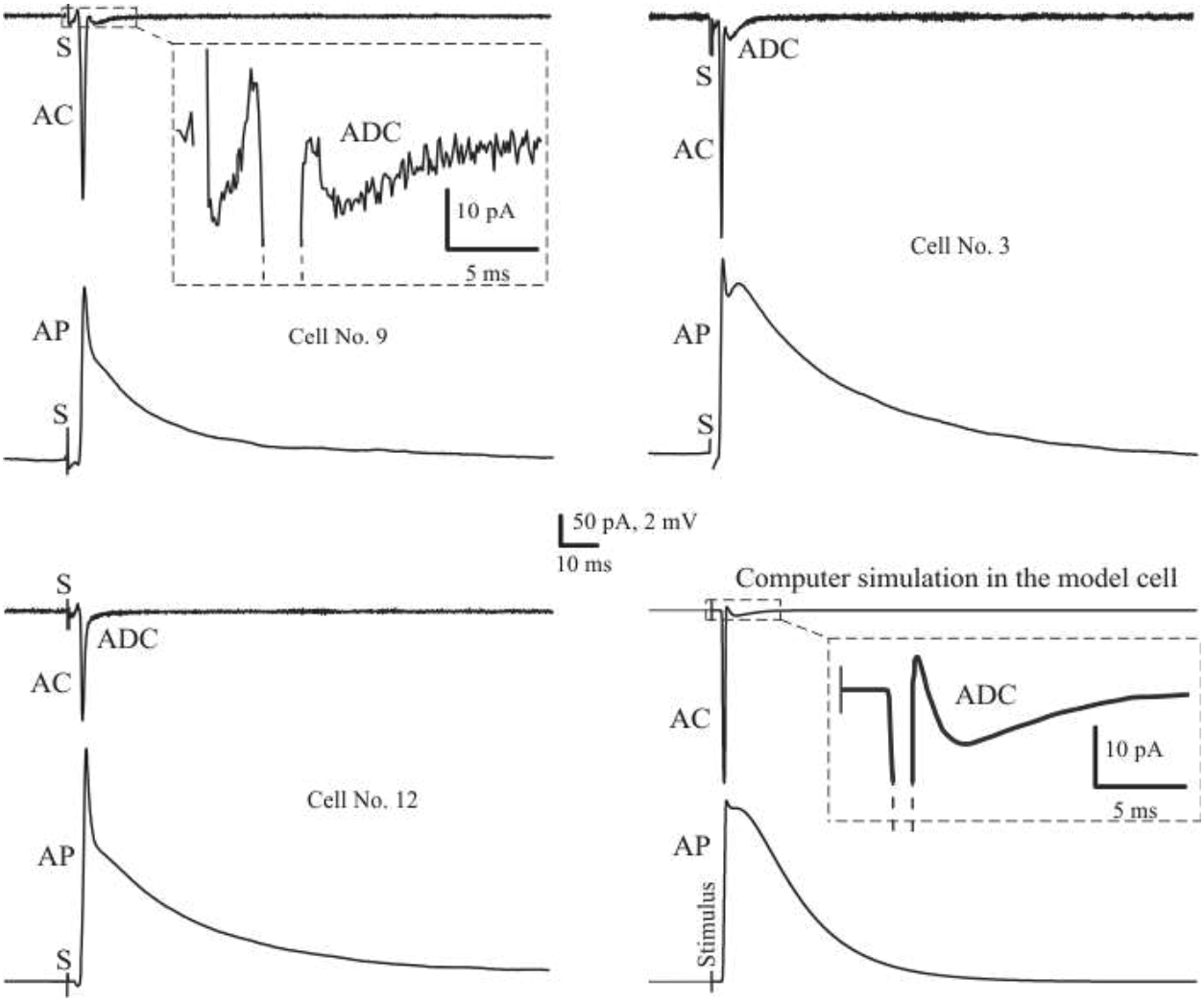


Fig 3. Recorded and modeled action currents (AC), potentials (AP), and afterdepolarizing currents (ADC). S – stimulation artifact.

Latency, amplitude, width of the action currents and potentials, amplitude and duration of the afterdepolarizing currents were measured. The results are listed in Table 1.

Table 1. The values of the parameters of recorded action currents, afterdepolarizing currents, and action potentials

No	Rat age, days	Latency, ms	A_{AC}, pA	AC, ms Width	A_{ADC}, pA	ADC, ms duration	A_{AP}, mV	AP, ms width
1	24	4.13	-382.5	0.662	-8.53	9.05	18.61	20.35
2	26	2.51	-324.8	0.653	-6.52	8.66	12.29	30.32
3	25	2.77	-379.8	0.578	-27.08	8.87	12.45	27.79
4	25	4.68	-103.8	0.661	0		7.26	13.35
5	17	3.28	-412	0.765	-22.07	8.63	9.681	25.27
6	17	2.69	-257.1	0.925	-7.02	6.3	9.128	38.62
7	21	5.06	-204.1	0.578	0		6.876	23.82
8	26	2.79	-379.5	0.703	-14.52	9.87	14.02	15.88
9	26	4.33	-311	0.638	-12.54	12.2	12.64	19.85
10	21	4.4	-293	0.697	-8.03	9.63	9.977	35.37
11	23	2.31	-288.1	0.947	0		21.2	15.88
12	22	4.1	-193.1	0.948	-9.53	9.23	14.64	11.55
Aver		**3.59**	**-294.1**	**0.73**	**-9.65**	**9.16**	**12.4**	**23.17**
SE		**0.28**	**26,6**	**0.04**	**2.45**	**0.51**	**1.24**	**2.49**

Mean amplitude and width of the action currents and potentials are equal to A_{AC} = -294 ± 27 pA, AC_width = 0.73 ± 0.04 ms, A_{AP} = 12.4 ± 1.24 mV, AP_width = 23.17 ± 2.49 ms (n = 12). Mean amplitude and duration of the afterdepolarizing currents are equal to A_{ADC} = -9.65 ± 2.45 pA, ADC_duration = 9.16 ± 0.51 ms (n = 12). Mean latency of the response is equal to t_{lat} = 3.59 ± 0.28 ms. The velocities of propagation of action potentials in the parallel fibers 0.206 ± 0.007 m/s at 22° C, 0.316 ± 0.007 m/s at 37° C, measured in our earlier work Baginskas et al. (2009), let us calculate an average distance of the stimulating electrode from the soma to be equal to $l_{avr} = 3.59 \cdot 10^{-3}$ s · 0.21 m/s = 0.754 m = 754 μm (coincides with the estimation by eye).

Modeling of action currents and potentials

The modeled action current was fitted to the recorded one by changing the two model parameters – maximal density of the fast sodium conductance $g_{Na,\max}$, and maximal density of the delayed rectifier potassium conductance $g_{K,\max}$. The results of modeling with $g_{Na,\max}$ = 81 mS/cm^2, $g_{K,\max}$ = 45 mS/cm^2, and the resurgent sodium conductance comprising 1% of the fast sodium conductance, i. e. $g_{NaR,\max} = 0.01 \cdot g_{Na,\max}$, are shown in Figure 4 at the room (22^o C) and physiological (37^o C) temperatures.

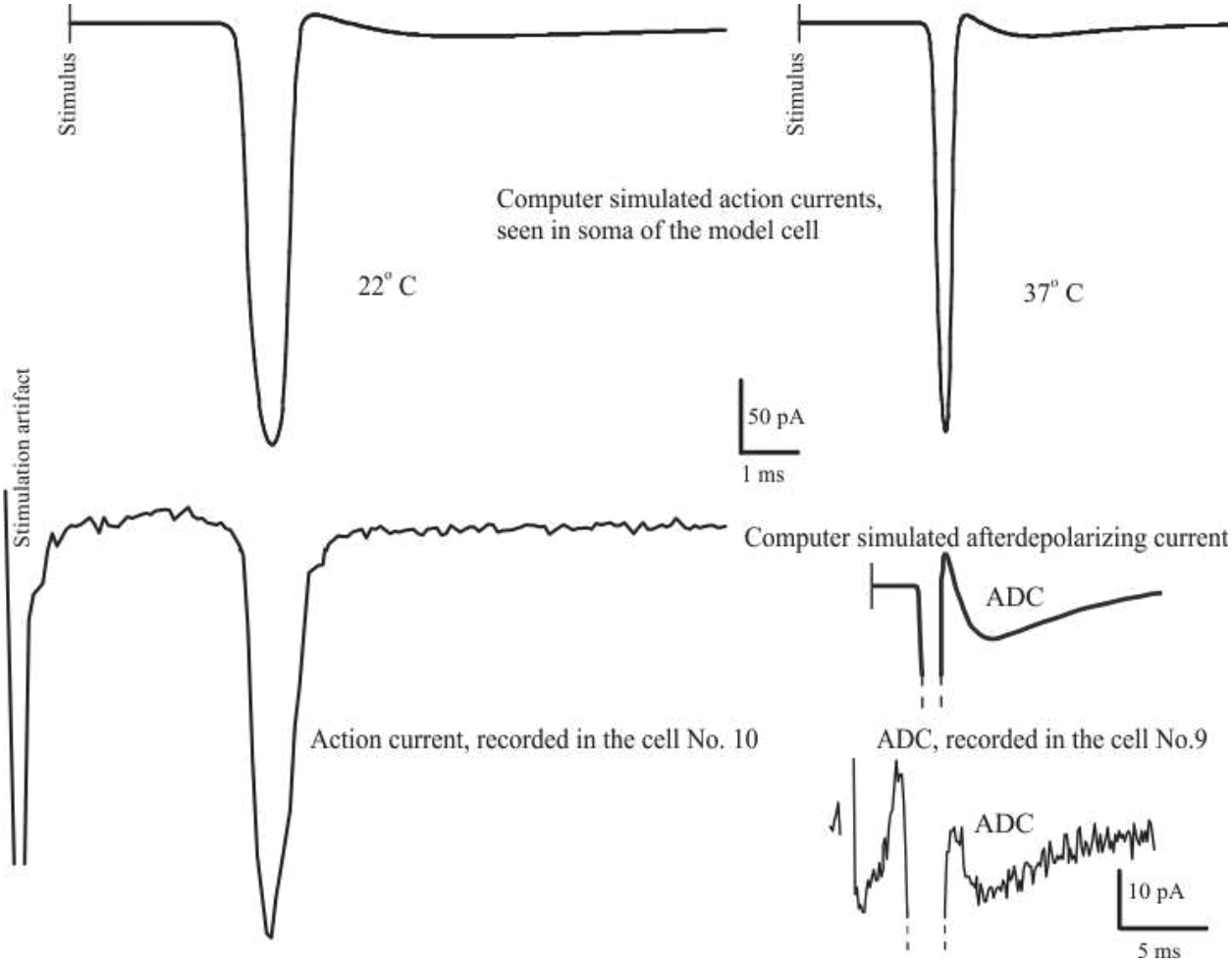


Fig 4. Match between the recorded and modeled action and afterdepolarizing currents. It is also shown modeled action current at 37^o C.

Values of the modelled action current are equal to -293 pA (amplitude), 0.74 ms (width), 3.51 ms (latency), 0.214 m/s (velocity) at 22° C; and -284 pA (amplitude), 0.275 ms (width), 2.477 ms (latency), 0.306 m/s (velocity) at 37° C. Values of the modelled afterdepolarizing current are equal to -9.03 pA (amplitude), 10.24 ms (duration). The modeled values match well the experimentally determined mean values (see Table 2).

Table 2. Correspondence between the modelled and recorded action and afterdepolarizing currents

Action current	A_{AC}, pA	Width, ms	Latency, ms	Velocity, m/s (22° C)	Velocity, m/s (37° C)	A_{ADC}, pA	ADC, ms duration
Model	-293	0.74	3.51	0.214	0.306	-9.03	10.24
Experiment	-294±27	0.73±0.04	3.59±0.28	0.206±0.007	0.316±0.007	-9.65±2.45	9.16±0.5

For computer simulation of the recorded action potentials we have to presume that the recording site is imperfect. Seal resistance R_{seal} of the fair whole cell patch clamp can be ~1 GΩ, and the recording system capacitance C_{elec} can be as large as 15 pF, in the case of fail of compensation procedure. The imperfect recording site is modeled by RC circuit consisting of R_{seal} and C_{elec} connected in parallel. The recording site RC circuit connects in parallel to the soma RC circuit. The combined soma-recording site RC circuit is equivalent to the soma having the membrane electrical parameters equal to R_m = 1700 Ω·cm^2, C_m = 8.5 μF/cm^2. This combined soma-recording site RC circuit filters incoming action potentials, lowering their amplitude and increasing their duration. At the values of R_{seal} = 1.14 GΩ, and C_{elec} = 11.5 pF, the filtering effect of the soma-recording site RC circuit gets large enough to make amplitude of action potentials less than 20 mV and width around 20 ms, matching the parameters of the recorded action potentials (see Fig. 5 and Table 3).

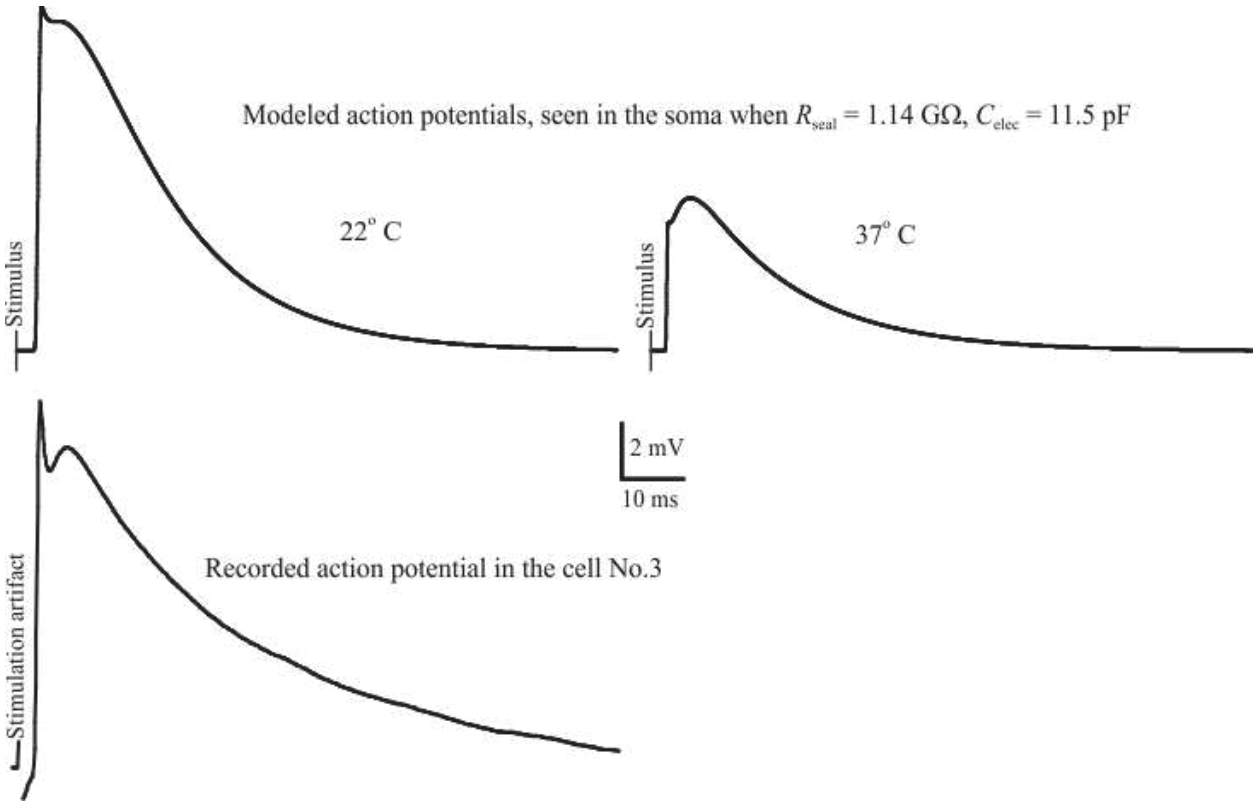


Fig 5. Match between the recorded and modeled action potentials. The soma-recording site RC circuit filters them so much that they look very unlike to the normal action potentials. The filtering effect is larger at 37° C than at 22° C, because of faster (narrower) transience of action current at higher temperature.

Table 3. Correspondence between the modelled and recorded action potentials

Action potential	Amplitude, mV	Width, ms
Model	12.33	19.64
Experiment	12.4 ± 1.24	23.2 ± 2.5

It is known from physics that RC circuits exert larger filtering effect on the faster (narrower) transience. Transience of the action currents is faster (narrower) at physiological temperature (37° C) than at room temperature (22° C). So, the action potentials generated by the action currents are filtered by the soma-recording site RC circuit more at 37° C than at 22° C, and the modelling confirm that (Figs 5, 6). The amplitude of modeled action potential at 37° C 5.48 mV is more than 2 times smaller than the amplitude at 22° C.

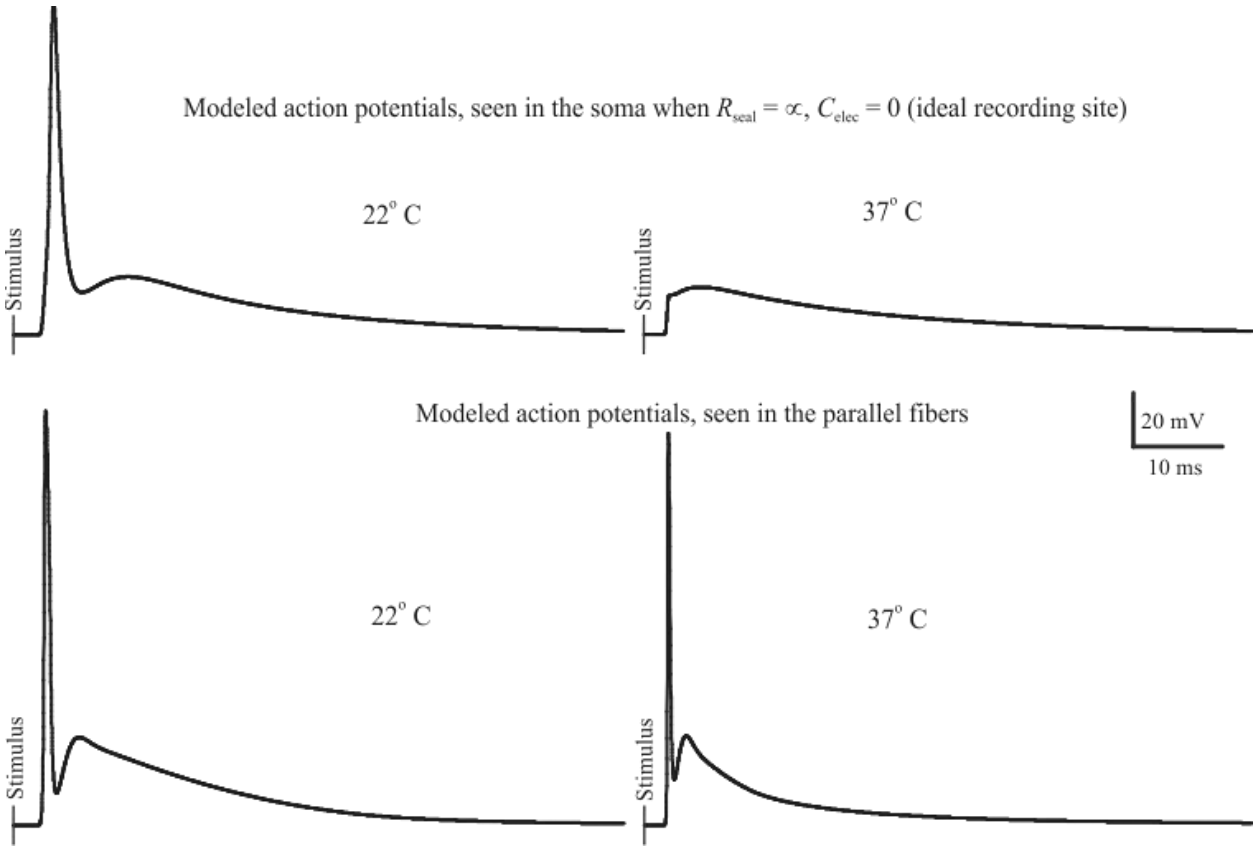


Fig 6. Modeled action potentials seen in the soma, and in the parallel fibers at temperatures of 22° C and 37° C. Unfiltered action potentials are seen in the parallel fibers (lower traces). The soma filters action potentials, decreasing their amplitude, and broadening their width (upper traces). Soma filtering effect is larger at 37° C than at 22° C, because of faster (narrower) transience of action current at higher temperature.

Even if the recording site is ideal, i. e. $R_{seal} = \infty$ and $C_{elec} = 0$ (fully compensated), soma alone exerts the filtering effect that can be large enough to substantially decrease the amplitude and increase the width of action potentials, especially at the physiological temperature due to the faster (narrower) transience of action current. As the modeling shows (Fig. 6, upper traces), the amplitude and width of action potentials seen in the soma at 22° C are equal to 122 mV, 1.30 ms, and seen at 37° C are equal to 17.7 mV, 20.8 ms. The similar reasoning suggests that action potentials in the parallel fibers have to have a higher amplitude and narrower width than those

seen in the soma due to absence in the parallel fibers of soma filtering effect. As the modeling shows (Fig. 6, lower traces), the amplitude and width of action potentials seen in the parallel fibers are equal to 153 mV, 0.70 ms at 22° C, and 144 mV, 0.32 ms at 37° C.

One more experimental evidence reproduced by the model is the ability of parallel fibers to transmit *in vivo* long trains up to 20 spikes at high (~1 kHz) frequency (Fig. 7).

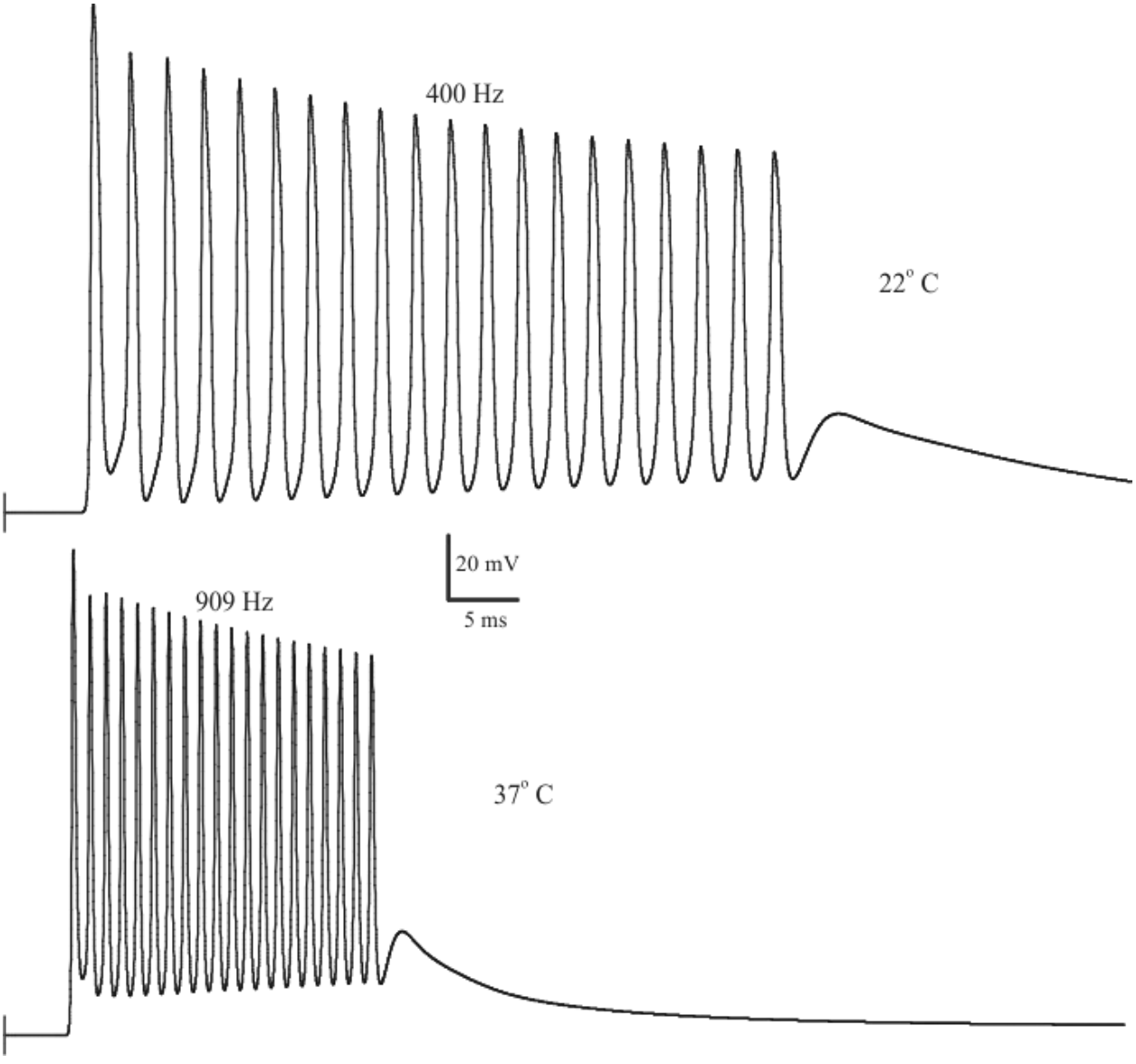


Fig 7. The highest frequency of action potentials transmitted without failing in the model parallel fibers.

The highest frequency of action potentials with no failing sustained by the parallel fibers is equal to 400 Hz at 22º C, and 909 Hz at 37º C.

The resurgent sodium current can be excluded from the model cell and the action currents and potentials calculated without this current, and then compared to the action currents and potentials with the intact resurgent sodium current (Fig. 8).

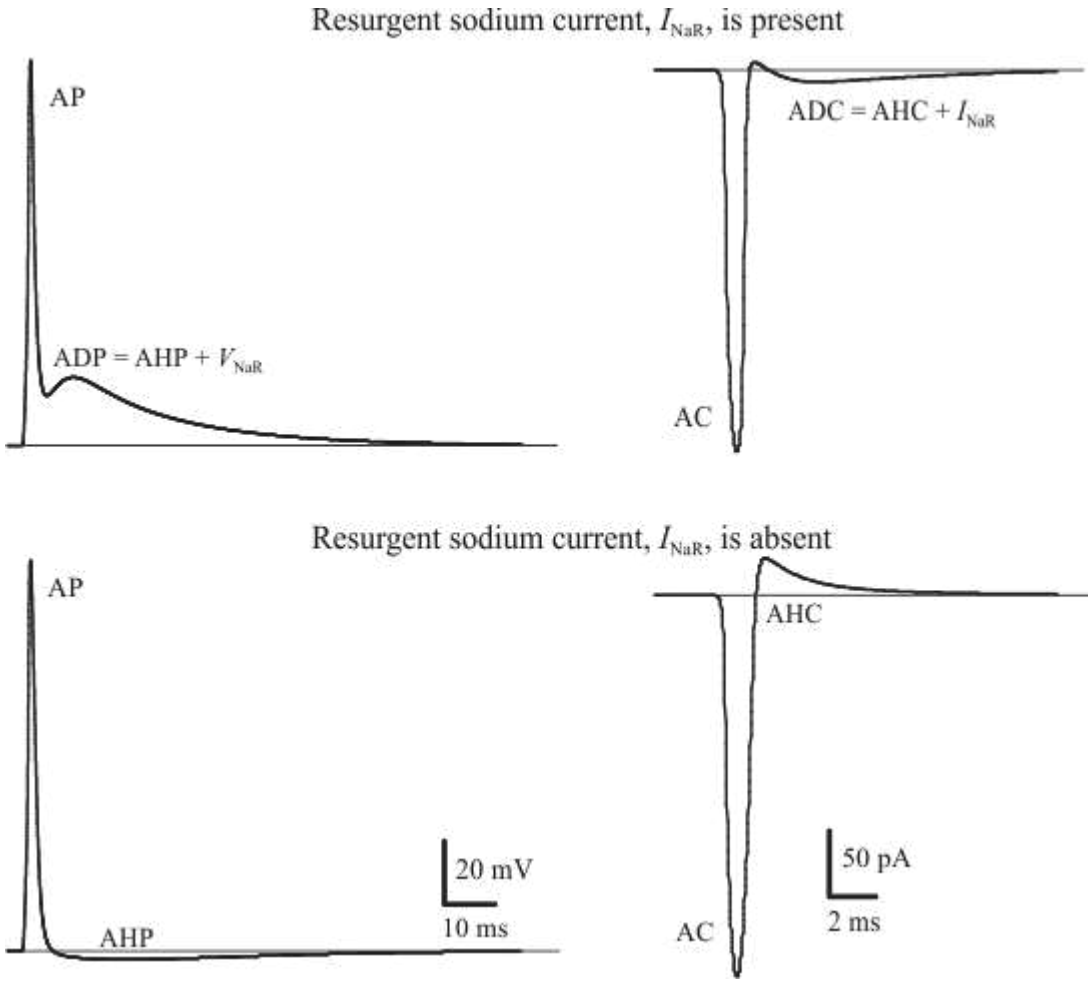


Fig 8. Modeled action potentials (AP) and action currents (AC) in the presence and absence of the resurgent sodium current, I_{NaR}. ADP – afterdepolarization potential, AHP – afterhyperpolarization potential, ADC – afterdepolarizing

current, AHC – afterhyperpolarizing potential, V_{NaR} – potential generated by the resurgent sodium current. ADC is sum of AHC and I_{NaR}. ADP is sum of AHP and V_{NaR}.

The comparison shows that the afterdepolarizing current (ADC) is sum of two factors – the resurgent sodium current, and delayed rectifier potassium current, responsible for the fast afterhyperpolarization. The afterdepolarization (ADP) is sum of depolarization, caused by the resurgent sodium current, and afterhyperpolarization, caused by the delayed rectifier potassium current.

Model estimation of Na^+ and K^+ intra-axonal concentration change

The change of sodium, Δc_{Na+}, and potassium, Δc_{K+}, ion concentrations in the parallel fibers due to propagation of action potentials has been calculated in the model cell. Single action potential leads to Δc_{Na+} = 0.99 mM, Δc_{K+} = -1.09 mM at 22° C, and Δc_{Na+} = 0.57 mM, Δc_{K+} = -0.66 mM at 37° C. These are not appreciable values to affect biochemical and electrical processes in the cell. Trains of 20 action potentials regularly registered in the cerebellar granule cells *in vivo* lead to Δc_{Na+} = 27.63 mM, Δc_{K+} = -28,01 mM at 22° C, and Δc_{Na+} = 13.69 mM, Δc_{K+} = -14,08 mM at 37° C, which are already appreciable values to affect biochemical and electrical processes in the cell. Below is shown a dependence of the concentration change on the number of spikes in the train with the inter-spike intervals of 5 ms.

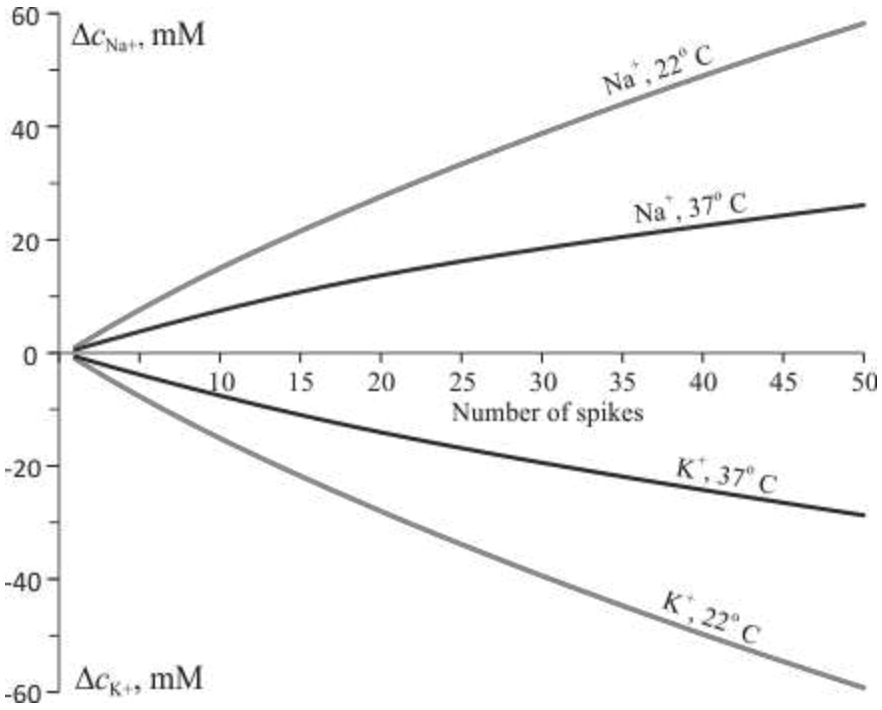


Fig 9. Dependence of the change of Na^+ and K^+ concentrations (Δc_{Na+}, Δc_{K+}) on the number of spikes in the train.

Excess of the sodium ions is removed by the sodium-potassium pump (Na^+/K^+-ATPase). However, kinetics of the pump is in the range of seconds, at least of decimal parts of second, and does not influence appreciably sodium and potassium ion concentration during even such long trains as 50 spikes. The results of modelling confirm this. Figure 10 shows an increase of sodium ion concentration during the train of 50 spikes with inter-spike intervals of 5 ms, and subsequent decrease of the concentration due to working of the sodium-potassium pump.

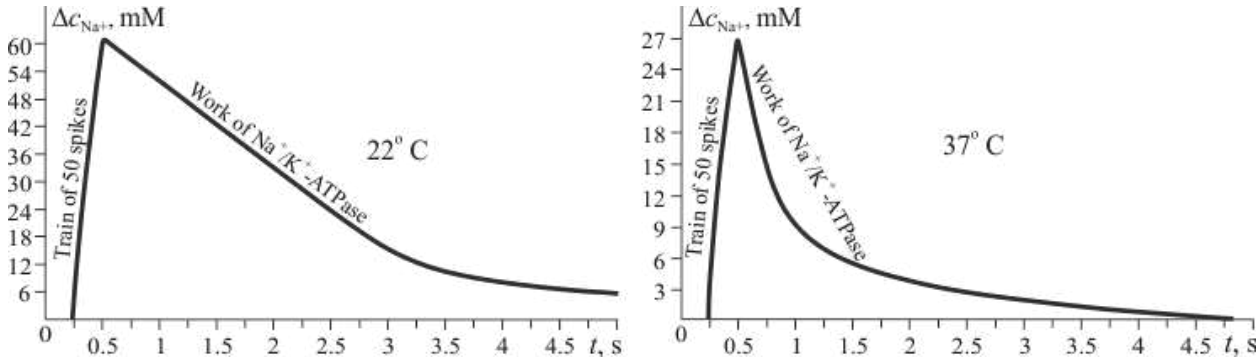


Fig. 10. Increase of the sodium concentration (Δc_{Na+}) during the train of 50 spikes, and subsequent decrease due to working of the sodium pump.

Theoretical estimation of the lower limit of Na^+ intra-axonal concentration increase

If one approximates the action current and potential with the rectangular pulse, and makes assumption that only sodium ions flow during the pulse, it is possible to estimate theoretically a lower limit of the sodium ion intra-axonal concentration change caused by the propagation of action potential. The assumption, of course, is rough. Really, during the transience of action current both types of ions flow. However, in some cases this theoretical method may be useful, because it lets quickly get the rough estimation of Na^+ concentration change in axons.

Let us consider rectangular sodium current pulse of amplitude A_c, and duration Δt_p that propagates along an axon with a velocity v (Fig. 11).

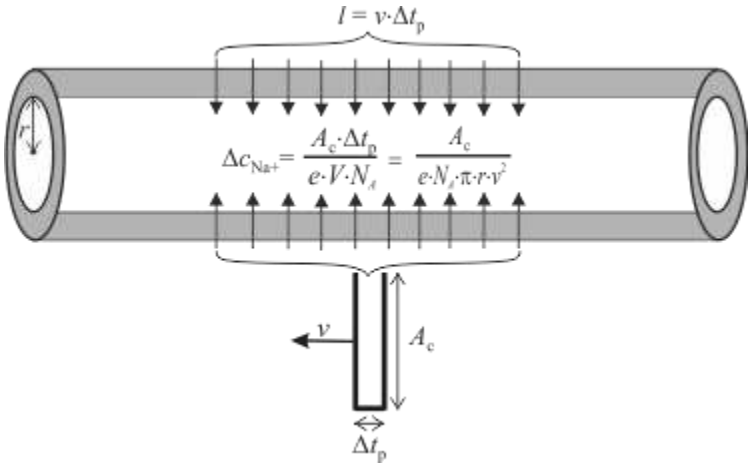


Fig. 11. Simplified model of propagation of action current along an axon. A_c – amplitude of action current pulse, Δt_p – duration of action current pulse, v – velocity of propagation of action current, r – radius of axon, l – distance traveled by the current pulse during its duration, $V = v \cdot \Delta t_p \cdot \pi \cdot r^2$ – volume over which sodium ions, carried by the current, distribute.

During the time period Δt_p current pulse travels the distance $l = v \cdot \Delta t_p$. The sodium ions spread over this distance entering the intra-axonal volume $V = l \cdot \pi \cdot r^2 = v \cdot \Delta t_p \cdot \pi \cdot r^2$. Number of ions N entering the axon is equal to the electric charge carried by the current pulse divided by the elementary charge, i. e. $N = A_c \cdot \Delta t_p / e$. An increase of sodium ion concentration is equal to $\Delta c_{Na+} = N/V$. By dividing this expression with the Avogadro number one gets concentration value in units of moles per volume unit. Thus, the increase of Na^+ concentration inside an axon is given by the equality

$$\Delta c_{Na+} = \frac{A_c}{e \cdot N_A \cdot \pi \cdot r^2 \cdot v}, \frac{\text{mol}}{(\text{units of volume})}, \tag{7}$$

where Δc_{Na+} is increase of Na^+ concentration inside an axon due to propagation of action potential, A_c – amplitude of the action current, e – elementary charge ($1.6 \cdot 10^{-19}$ C), N_A – Avogadro number ($6.022 \cdot 10^{23}$ 1/mol), r – radius of the axon, v – velocity of propagation of action potential.

Substituting into this equation values of the quantities from the experiment $A_c = 294$ pA, $v = 0.21$ m/s, $r = 0.1$ μm, we get $\Delta c_{Na+} = 0.46$ mM, which is two times less than the model evaluated increase. This discrepancy indicates that potassium ions constitute appreciable part of the modeled action current (this, of course, is the case in reality, too).

Eq. 7 is useless if action potentials, not currents, are recorded in the experiments. However, the equation for action potentials can be derived in a similar way.

The change of sodium ion concentration is equal to $\Delta c_{Na+} = N/V$, where N is number of sodium ions entering an axon, $V = v \cdot \Delta t_p \cdot \pi \cdot r^2$ is volume into which these ions enter (v is velocity of propagation of action potential, Δt_p – duration of the rectangular pulse of potential, r – is

radius of axon). Membrane area embraced by this volume $S_m = v \cdot \Delta t_p \cdot 2 \cdot \pi \cdot r$ is charged to the voltage equal to the amplitude of action potential A_p. The electrical charge needed for that is equal to $q = C_m \cdot S_m \cdot A_p$, where $C_m = 1$ μF/cm^2 is specific membrane capacitance. Substituting the expression for S_m one gets $q = v \cdot \Delta t_p \cdot 2 \cdot \pi \cdot r \cdot C_m \cdot A_p$. Since $N = q/e$, the increase of Na^+ concentration inside an axon is given by the equality:

$$\Delta c_{Na+} = \frac{2 \cdot C_m \cdot A_p}{e \cdot N_A \cdot r}, \frac{\text{mol}}{(\text{units of volume})}, \tag{8}$$

where Δc_{Na+} is increase of Na^+ concentration inside an axon due to propagation of action potential, A_p – amplitude of the action potential, C_m – specific membrane capacitance, r – radius of axon, e – elementary charge, N_A – Avogadro number.

Substituting into equation the value of $A_p = 144$ mV from the modeling at 37° C, we get $\Delta c_{Na+} = 0.3$ mM, which is again almost two times less, than modeled increase at 37° C, indicating that potassium ions constitute appreciable part of the real action current.

Discussion

Computer simulation of the recorded action currents are done by changing two model parameters – maximal density of the fast sodium conductance $g_{Na,max}$, and maximal density of the delayed rectifier potassium conductance $g_{K,max}$. When $g_{Na,max} = 81$ mS/cm^2, $g_{K,max} = 45$ mS/cm^2, and the resurgent part of sodium conductance constitutes 1% of the fast sodium conductance, i. e. $g_{NaR,max} = 0.01 \cdot g_{Na,max}$, the model current matches many of the experimental evidences – latency, amplitude, width of the current, duration and amplitude of the afterdepolarizing current (ADP),

velocities of propagation at 22° C and 37° C, and reproduce the ability of parallel fibers to transmit long trains of spikes at high, up to 1 kHz, frequency.

Computer simulation of the recorded action potentials is achieved only by including into the model the RC circuit of recording site consisting of the seal resistance R_{seal} = 1.14 GΩ and recording system capacitance C_{elec} = 11.5 pF, connected in parallel. This circuit connects in parallel to the soma RC circuit. The combined soma-recording site RC circuit filters incoming action potentials, lowering their amplitude till 12.3 mV and increasing their width till 19.6 mV. Modeling shows that even soma RC circuit alone can filter incoming action potentials substantially. For instance, action potential at 22° C is filtered only little, because of slower (wider) transience, and looks like normal action potential with the amplitude of 122 mV and width of 1.30 ms. The action potential at 37° C is filtered already substantially, because of faster (narrower) transience, and looks like abnormal action potential with the amplitude of 17.7 mV and width of 20.8 ms. Action potentials in the parallel fibers are of higher amplitude (153 mV at 22° C, 144 mV at 37° C) and of narrower width (0.7 ms at 22° C, 0.32 ms at 37° C) than the ones seen in the soma due to absence of soma filtering effect in the parallel fibers.

Modeling shows that frequency of action potentials transmitted by the parallel fibers can be as large as 400 Hz at 22° C, and 909 Hz at 37° C, corresponding to the experimental evidences (Jorntell and Ekerot, 2006; Rancz et al., 2007; van Beugen et al., 2013, Powell et al., 2015).

The modeled amplitude and duration of the afterdepolarizing current (ADC) -9 mV, 10 ms, and afterdepolarization potential (ADP) 22 mV, 100 ms correspond to the experimental results of the present work and of the others (Fatemeh et al., 2004; Lewis and Raman, 2014; Pekala et al., 2014; Raastad, 2019; Kamiva, 2019; Aman and Raman, 2024). The modeling suggests that ADC is sum of resurgent sodium current and delayed rectifier potassium current, and ADP is sum of

depolarization, caused by the resurgent sodium current, and afterhyperpolarization, caused by the delayed rectifier potassium current. This two-component feature of the ADC explains a large variability of ADC amplitude from cell to cell in our experiments (0-27 pA) and in the experiments of other researchers.

Modeling shows that the change of sodium (0.9 mM at 22° C, 0.57 mM at 37° C) and potassium (-1.09 mM at 22° C, -0.66 mM at 37° C) ion concentrations in the parallel fibers due to the propagation of a single action potential is not appreciable to affect biochemical and electrical processes in the cell. However, the change of concentrations during 20 spikes long trains (characteristic for the cerebellar granule cells) is already appreciable (27.63 mM at 22° C, 13.69 mM at 37° C, and -28,01 mM at 22° C, -14,08 mM at 37° C) to do this. Na^+/K^+-ATPase is not fast enough to remove excess of sodium ions quickly. Kinetics of the sodium pump is in the range of seconds, at least of decimal parts of second (Karlish and Yates 1978; Lupfert et al. 2001; Artigas and Gadsby 2002).

Shortly about what can be of interest for neurophysiologists:

Conclusions

1. The features of modeled action currents and potentials match many of the features of recorded ones when maximal density of the fast sodium conductance in the cerebellar parallel fibers is equal to 81 mS/cm^2, maximal density of delayed rectifier potassium conductance is equal to 45 mS/cm^2, and the density of resurgent sodium conductance comprises 1% of the fast sodium conductance.

2. Modeling shows that the action potentials recorded in the soma are distorted due to the filtering effect of soma-recording site RC circuit.

3. Modeling shows that the afterdepolarizing current (ADC) is a sum of resurgent sodium current and delayed rectifier potassium current, and the afterdepolarization potential (ADP) is a sum of depolarization, caused by the resurgent sodium current, and afterhyperpolarization, caused by the delayed rectifier potassium current.

4. Increase of sodium ion concentration in the parallel fibers during the propagation of 20 spikes long trains is large enough to affect biochemical and electrical processes in the cell.

5. The formulas were derived that let one to estimate theoretical lower limit of Na^+ concentration increase in axons due to propagation of action potentials.

Acknowledgements

References

Afshari, F. S., Ptak, K., Khaliq, Z. M., Grieco, T. M., Slater, N. T., McCrimmon, D. R., Raman, I. M. (2004). Resurgent Na currents in four classes of neurons of the cerebellum. Journal of Neurophysiology, 92(5), 831-843. https://doi.org/10.1152/jn.00261.2004

Aman, T. K., Raman, I. M. (2024). Resurgent current in context: Insights from the structure and function of Na and K channels. Biophysical Journal, 123(14), 1924-1941, https://doi.org/10.1016/j.bpj.2023.12.016

Arleo, A., Nieus, T., Bezzi, M., D'Errico, A., D'Angelo, E., Coenen, O. J.-M. D. (2010). How Synaptic Release Probability Shapes Neuronal Transmission: Information-Theoretic Analysis in a Cerebellar Granule Cell. Neural Computation, 22 (8), 2031–2058. https://doi.org/10.1162/NECO_a_00006-Arleo

Artigas, P., Gadsby, D. C. (2002). Ion channel-like properties of the Na+/K+ Pump. Annals of the New York Academy of Sciences, 976, 31-40. https://doi.org/10.1111/j.1749-6632.2002.tb04711.x

Baginskas, A., Palani, D., Chiu, K., Raastad, M. (2009). The H-current secures action potential transmission at high frequencies in rat cerebellar parallel fibers. European Journal of Neuroscience, 29(1), 87-96. https://doi.org/10.1111/j.1460-9568.2008.06566.x

Chen, W-H., Chu, K-C., Wu, S-J., Wu, J-C., Shui, H. A. and Wu, M-L. (1999). Early metabolic inhibition-induced intracellular sodium and calcium increase in rat cerebellar granule cells. Journal Physiology, 515.1, 133–146. https://doi.org/10.1111/j.1469-7793.1999.133ad.x

Chizhov, A. V., Amakhin, D. V., Zaitsev, A. V. (2019). Mathematical model of Na-K-Cl homeostasis in ictal and interictal discharges. PLoS ONE, 14(3), e0213904. https://doi.org/10.1371/journal.pone.0213904

Diwakar, S., Magistretti, J., Goldfarb, M., Naldi, G., D'Angelo, E. (2009). Axonal Na^+ channels ensure fast spike activation and back-propagation in cerebellar granule cells. Journal of Neurophysiology, 101(2), 519-532. https://doi.org/10.1152/jn.90382.2008

Dover, K., Marra, C., Solinas, S., Popovic, M., Subramaniyam, S., Zecevic, D., D'Angelo, E., Goldfarb, M. (2016). FHF-independent conduction of action potentials along the leak-resistant cerebellar granule cell axon. Nature Communications, 7, 12895. https://doi.org/10.1038/ncomms12895

Fang, X., Duan, S., and Wang, L. (2021). Memristive Hodgkin-Huxley Spiking Neuron Model for Reproducing Neuron Behaviors. Frontiers in Neuroscience, 15, 730566. https://doi.org/10.3389/fnins.2021.730566

Fatemeh, A. S., Ptak, K., Khaliq, Z. M., Grieco, T. M., Slater, N. T., McCrimmon, D. R., and Raman, I. M. (2004). Resurgent Na Currents in Four Classes of Neurons of the Cerebellum. Journal of Neurophysiology, 92(5), 2831-2843. https://doi.org/10.1152/jn.00261.2004

Fohlmeister, J. F. (2015). Voltage gating by molecular subunits of Na+ and K+ ion channels: higher-dimensional cubic kinetics, rate constants, and temperature. Journal of Neurophysiology, 113(10), 3759-3777. https://doi.org/10.1152/jn.00551.2014

Gerstner, W., Kistler, W. M., Naud, R., Paninski, L. (2014). Neuronal Dynamics. From single neurons to networks and models of cognition (online book). https://neuronaldynamics.epfl.ch/online/Ch2.S2.html

Gundappa-Sulur, G., De Schutter, E., Bower, J. M. (1999). Ascending granule cell axon: an important component of cerebellar cortical circuitry. The Journal of Comparative Neurology, 408(4), 580-596. https://doi.org/10.1002/(SICI)1096-9861(19990614)408:4<580::AID-CNE11>3.0.CO;2-O

Huang, C. M., Wang, L., Huang, R. H. (2006). Cerebellar granule cell: ascending axon and parallel fiber. European Journal of Neuroscience 23(7), 1731-1737. https://doi.org/10.1111/j.1460-9568.2006.04690.x

Jörntell, H., Ekerot, C. F. (2006). Properties of somatosensory synaptic integration in cerebellar granule cells in vivo. Journal of Neuroscience, 26(45), 11786-11797. https://doi.org/10.1523/JNEUROSCI.2939-06.2006

Kamiya, H. (2019). Excitability Tuning of Axons by Afterdepolarization. Frontiers in Cellular Neuroscience, 13, 407. https://doi.org/10.3389/fncel.2019.00407

Karlish, S. J. D., Yates, D. W. (1978). Tryptophan fluorescence of (Na^+K^+)-ATPase as a tool in the study of the enzyme mechanism. Biochimica et Biophysica Acta, 527, 115-130. https://doi.org/10.1016/0005-2744(78)90261-9

Lewis, A. H., Raman, I. M. (2014). Resurgent current of voltage-gated Na+ channels. The Journal of Physiology, 592.22, 4825–4838. https://physoc.onlinelibrary.wiley.com/doi/epdf/10.1113/jphysiol.2014.277582

Liu, Z., Golowasch, J., Marder, E., Abbott, L. F. (1998). A Model Neuron with Activity-Dependent Conductances Regulated by Multiple Calcium Sensors. Journal of Neuroscience, 18(7), 2309–2320. https://doi.org/10.1523/JNEUROSCI.18-07-02309.1998

Lüpfert, C., Grell, E., Pintschovius, V., Apell, H. J., Cornelius, F., Clarke, R. J. (2001). Rate limitation of the Na(+),K(+)-ATPase pump cycle. Biophysical Journal, 81(4), 2069-2081. https://doi.org/10.1016/S0006-3495(01)75856-0

Magistretti, J., Castelli, L., Forti, L., D'Angelo, E. (2006). Kinetic and functional analysis of transient, persistent and resurgent sodium currents in rat cerebellar granule cells in situ: an electrophysiological and modelling study. The Journal of Physiology, 573.1, 83-106. https://doi.org/10.1113/jphysiol.2006.106682

Masoli, S., Rizza, M. F., Sgritta, M., Van Geit, W., Schürmann, F. and D'Angelo, E. (2017). Single Neuron Optimization as a Basis for Accurate Biophysical Modeling: The Case of Cerebellar Granule Cells. Frontiers in Cellular Neuroscience, 11, 71. https://doi.org/10.3389/fncel.2017.00071

Masoli, S., Tognolina, M., Laforenza, U., Moccia, F., D'Angelo, E. (2020). Parameter tuning differentiates granule cell subtypes enriching transmission properties at the cerebellum input stage. Communications Biology, 3(1), 222. https://doi.org/10.1038/s42003-020-0953-x

Ono, Y., Ojima, K., Torii, F., Takaya, E., Doi, N., Nakagawa, K., Hata, S., Abe, K., Sorimachi, H. (2010). Skeletal muscle-specific calpain is an intracellular Na^+-dependent protease. Journal of Biological Chemistry, 285(30), 22986-22998. https://doi.org/10.1074/jbc.M110.126946

Osorio, N., Alcaraz, G., Padilla, F., Couraud, F., Delmas, P., Crest, M. (2005) Differential targeting and functional specialization of sodium channels in cultured cerebellar granule cells. The Journal of Physiology, 569(Pt 3), 801-816. https://doi.org/10.1113/jphysiol.2005.097022

Page, M. J., and Di Cera, E. (2006). Role of Na^+ and K^+ in Enzyme Function. Physiological Reviews, 86, 1049-1092. https://doi.org/10.1152/physrev.00008.2006

Pekala, D., Baginskas, A., Szkudlarek, H. J., Raastad, M. (2014). Components of action potential repolarization in cerebellar parallel fibres. The Journal of Physiology, 592(22), 4911-4929. https://doi.org/10.1113/jphysiol.2014.280719

Pichitpornchai, C., Rawson, J. A., Rees, S. (1994) Morphology of parallel fibres in the cerebellar cortex of the rat: an experimental light and electron microscopic study with biocytin. Journal of Comparative Neurology, 342(2), 206-220. https://doi.org/10.1002/cne.903420205

Polder, H. R., Weskamp, M., Linz, K., Meyer, R. (2005). Voltage-Clamp and Patch-Clamp Techniques. In: Dhein, S., Mohr, F. W., Delmar, M. (eds) Practical Methods in Cardiovascular Research. Springer, Berlin, Heidelberg. https://doi.org/10.1007/3-540-26574-0_16

Powell, K., Mathy, A., Duguid, I., Hausser, M. (2015). Synaptic representation of locomotion in single cerebellar granule cells. Elife, 4, e07290, 1-18. https://doi.org/10.7554/eLife.07290

Raastad M. (2019). The Slow Depolarization Following Individual Spikes in Thin, Unmyelinated Axons in Mammalian Cortex. Frontiers in Cellular Neuroscience, 13, 203. https://doi.org/10.3389/fncel.2019.00203

Rancz, E. A., Ishikawa, T., Duguid, I., Chadderton, P., Mahon, S., Häusser, M. (2007). High-fidelity transmission of sensory information by single cerebellar mossy fibre boutons. Nature, 450(7173), 1245-1248. https://doi.org/10.1038/nature05995

Schaller, K. L., Caldwell, J. H. (2003). Expression and distribution of voltage-gated sodium channels in the cerebellum. Cerebellum, 2 (1), 2-9. https://doi.org/10.1080/14734220309424

Sigworth, F. J. (1995). Design of the EPC-9, a computer-controlled patch-clamp amplifier. 1. Hardware. Journal of Neuroscience Methods, 56(2), 195-202. https://doi.org/10.1016/0165-0270(94)00128-4

Sterratt, D. C. (2015). Q10: the Effect of Temperature on Ion Channel Kinetics. In D. Jaeger, & R. Jung (Eds.). Encyclopedia of Computational Neuroscience, 2551-2552. Springer. https://doi.org/10.1007/978-1-4614-6675-8_236

Su, M., Kakita, A., Yamada, M., Takahashi, H., Ikuta, F. (1996). Degeneration of the synaptic boutons of parallel fibers in rats treated with methylmercury: Chronological observations. Neuropathology, 16(3), 172-177. https://doi.org/10.1111/j.1440-1789.1996.tb00178.x

Tigerholm, J., Petersson, M. E., Obreja, O., Eberhardt, E., Namer, B., Weidner, C., Lampert, A., Carr, R. W., Schmelz, M., Fransén, E. (2015). C-Fiber Recovery Cycle Supernormality Depends on Ion Concentration and Ion Channel Permeability. Biophysical Journal, 108 (5), 1057-1071. https://doi.org/10.1016/j.bpj.2014.12.034

van Beugen, B. J., Gao, Z., Boele, H. J., Hoebeek, F., De Zeeuw, C. I. (2013). High frequency burst firing of granule cells ensures transmission at the parallel fiber to purkinje cell synapse at the cost of temporal coding. Frontiers in Neural Circuits, 7, 95. https://doi.org/10.3389/fncir.2013.00095

Wang, T., Arcos, D., Doty, D. F., Pettitt, M. B., Iwahara, J. (2025) Strong field gradients enable NMR-based diffusion measurements for K^+, Mg^{2+}, Cl^-, and SO_4^{2-} ions in biomolecular solutions. Journal of Magnetic Resonance, 376, 107890. https://doi.org/10.1016/j.jmr.2025.107890

Wang, W., Touhara, K. K., Weir, K., Bean, B. P., MacKinnon, R. (2016). Cooperative regulation by G proteins and Na^+ of neuronal GIRK2 K^+ channels. eLife, 5, e15751. https://doi.org/10.7554/eLife.15751

Wasman, S. G. (2006). Axonal conduction and injury in multiple sclerosis: the role of sodium channels. Nature Reviews Neuroscience, 7, 932-941. https://doi.org/10.1038/nrn2023

Wen, Z., Boqiang, F., Divyansh, A., Tun, L., Yuguo, Y. (2019). Axonal sodium and potassium conductance density determines spiking dynamical properties of regular- and fast-spiking neurons. Nonlinear Dynamics, 95(5765). https://doi.org/10.1007/s11071-018-4613-3

Yu, X. M., Groveman, B. R., Fang, X. Q., Lin, S. X. (2010). The role of intracellular sodium (Na+) in the regulation of calcium (Ca2+)-mediated signaling and toxicity. Health, 2(1), 8-15. https://doi.org/10.4236/health.2010.21002

Zang, Y., Marder, E., Marom, S. (2023). Sodium channel slow inactivation normalizes firing in axons with uneven conductance distributions. Current Biology, 33(9), 1818-1824.e3. https://doi.org/10.1016/j.cub.2023.03.043

Zylbertal, A., Yarom, Y., and Wagner, S. (2017). The Slow Dynamics of Intracellular Sodium Concentration Increase the Time Window of Neuronal Integration: A Simulation Study. Frontiers in Computational Neuroscience, 11, 85. https://doi.org/10.3389/fncom.2017.00085